6. SITE 1047[1]

Shipboard Scientific Party[2]

HOLE 1047A

Position: 15°31.8344′N, 58°42.1909′W

Date occupied: 1530, 3 January 1997

Spud hole: 0115, 4 January 1997

End hole: 2115, 5 January 1997

Time on hole: 2 days, 5 hr, 45 min

Seafloor depth (drill-pipe measurement from rig floor, m): 5067

Distance between rig floor and sea level (m): 11.0

Water depth (drill-pipe measurement from sea level, m): 5056

Total depth (from rig floor, m): 5700

Penetration (m): 633

Total core recovered (m): 0

Comments: Logging while drilling (LWD). No coring done. Seafloor depth identified from LWD data.

Principal results: Located 1 km west of the deformation front, Site 1047 was drilled through the décollement zone and more than 300 m into the underthrust section of the northern Barbados accretionary prism. Site 1047 is a reoccupation of Site 676, which was cored to 310 m to document processes associated with the initiation of offscraping. At Site 1047, LWD gamma-ray, resistivity, density, caliper, photoelectric effect, and neutron porosity logs were acquired. Excluding neutron porosity, all logs are of excellent quality.

Traditional visual and multivariate statistical analyses define six log units (Fig. 1). Log Unit 1 (0–158 m below seafloor [mbsf]) is characterized by increasing density and resistivity with depth, which suggests a normal compaction trend and high photoelectric effect. These log signatures are consistent with a carbonate-rich lithologic unit that occurs over the same depth interval at Site 676. Log Unit 2 and Subunits 3a and 3b (158–276 mbsf) show a general decrease in resistivity, density, photoelectric effect, and gamma-ray values. These log responses reflect a downhole transition to an increasingly underconsolidated, clay-rich unit above the décollement zone. An interval of very low density, low resistivity, and low gamma-ray values defines log Subunit 3c (276–300 mbsf). This interval correlates with a lower Miocene radiolarian mudstone that includes mud-filled veins, a thrust fault, and a methane anomaly. This interval lies within the décollement zone at Site 676. An increase both in differential caliper in this interval and in torque on the drill bit suggest that the muddy section was extruding into the drill hole, perhaps because of overpressuring. Log Units 4 (300–493 mbsf) and 5 (493–562 mbsf) show a spiky nature throughout the photoelectric effect and gamma-ray logs, suggesting interbedding of dissimilar lithologies. Strong variation in resistivity in Unit 5 suggests sand interbeds, probably correlative to the turbidite sequence cored at Sites 671 and 672. Log Unit 6 (562–619 mbsf) is characterized by decreasing photoelectric effect and density and increasing and variable gamma-ray values. Log Unit 6 correlates with lower Eocene noncalcareous claystones and siliceous claystones recovered at Sites 672 and 543.

Comparison of the density curves from Site 1047 and reference Site 1044 shows selective consolidation in log Units 3 (décollement zone) and 5 (underthrust sandy turbidite section). Presumably, both intervals of localized consolidation are caused by dewatering in response to localized deformation and by loading resulting from underthrusting. A synthetic seismogram generated from the density log reproduces the negative polarity reflection from the décollement zone and the strong reflections from the underthrust turbidite sequence, but poorly matches reflections in the accretionary prism.

BACKGROUND AND OBJECTIVES

Site 1047 is located 1 km west of the location of initial offscraping of the accretionary prism (Fig. 2). Here, the accretionary prism forms by distributed shortening of the sedimentary section, with no discrete frontal thrust resolved from the seismic reflection data (Fig. 3). Seismic reflectors in the offscraping sequence lose continuity in this zone, apparently as a result of small-scale faulting. The seismic data indicate that the décollement zone is at about 300 mbsf and the oceanic crust is at about 850 mbsf. A sequence of high-amplitude, parallel, continuous reflectors between about 500 and 650 mbsf (Fig. 3) may represent the Oligocene and Eocene turbidite sequence cored at Site 672 (Shipboard Scientific Party, 1988a) and logged at Site 1044. Site 1047 is a reoccupation of Site 676, where the shipboard party recovered structural and stratigraphic evidence for small-scale thrust faulting and a weakly developed décollement zone (Shipboard Scientific Party, 1988b).

A primary objective of drilling at Site 1047 was to measure the physical properties of the décollement zone as it initially develops. Similarly, we planned to gauge the changes in physical properties of the offscraped sequence as it is subjected to distributed initial deformation. Another primary objective of drilling at Site 1047 was to penetrate the underthrust section through this turbidite sequence to determine its consolidation during the initial state of loading by the accretionary prism.

OPERATIONS

Hole 1047A

After the drill string was pulled clear of the seafloor following Hole 1046A, the vessel was offset in dynamic positioning mode to Site 1047, and a positioning beacon was deployed. During the move to Site 1047, the LWD tools were changed out. A request was made to the Ocean Drilling Program (ODP) to deepen the penetration at Site 1047 from the approved 500 mbsf to 650 mbsf. The deeper penetration was intended to obtain LWD data from the turbidite sequence in the underthrust section at a location between reference Site 1044 and Site 1046, farther west in the accretionary prism. ODP approved the request.

Hole 1047A was spudded at 0115 hr, 4 January 1997, at Global Positioning System (GPS) coordinates 15°31.8344′N, 58°42.1909′W. This location is ~29 m along an azimuth 150° from Site 676 of Leg 110. Drilling was initiated at 35 m/hr at a water depth of 5070 m be-

[1]Moore, J.C., Klaus, A., et al., 1998. *Proc. ODP, Init. Repts.*, 171A: College Station, TX (Ocean Drilling Program).

[2]Shipboard Scientific Party is given in the list preceding the Table of Contents.

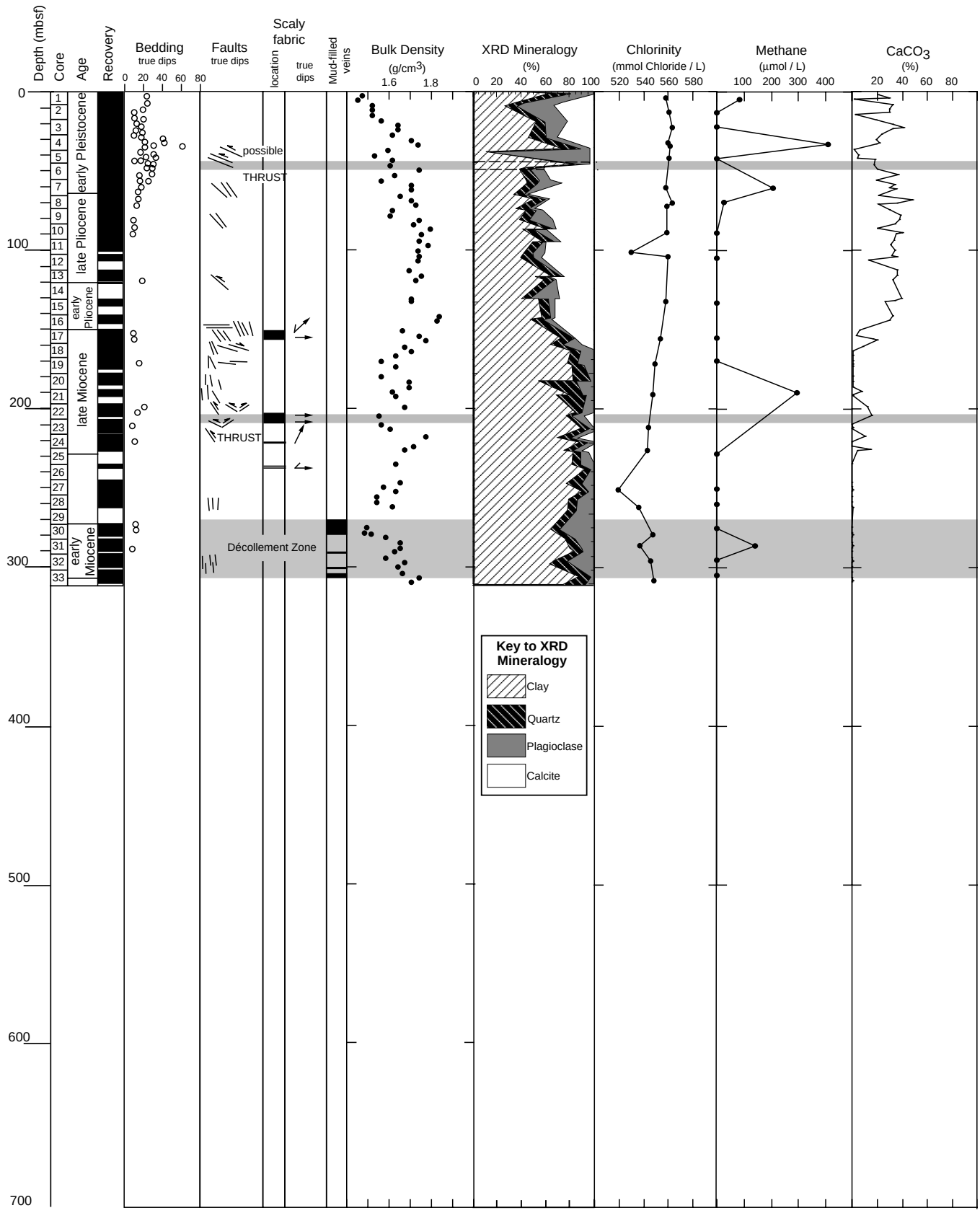

Figure 1. Summary of log data from Site 1047 and core data from Site 676. Log units for Hole 1047A are shown beside the lithologic units for Site 676. Shaded bars represent fault zones interpreted from Site 676 core and Site 1047 LWD data.

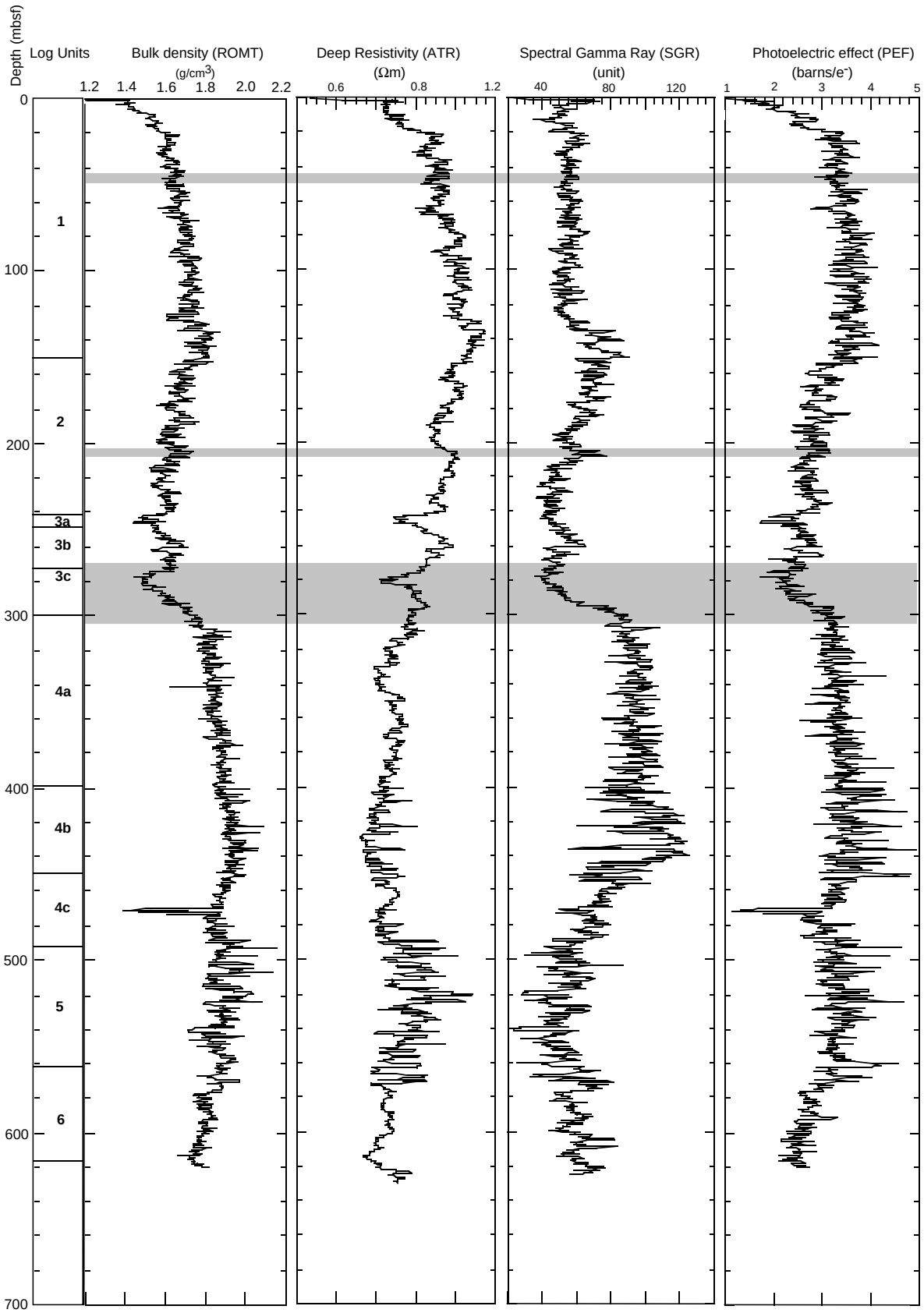

Figure 1 (continued).

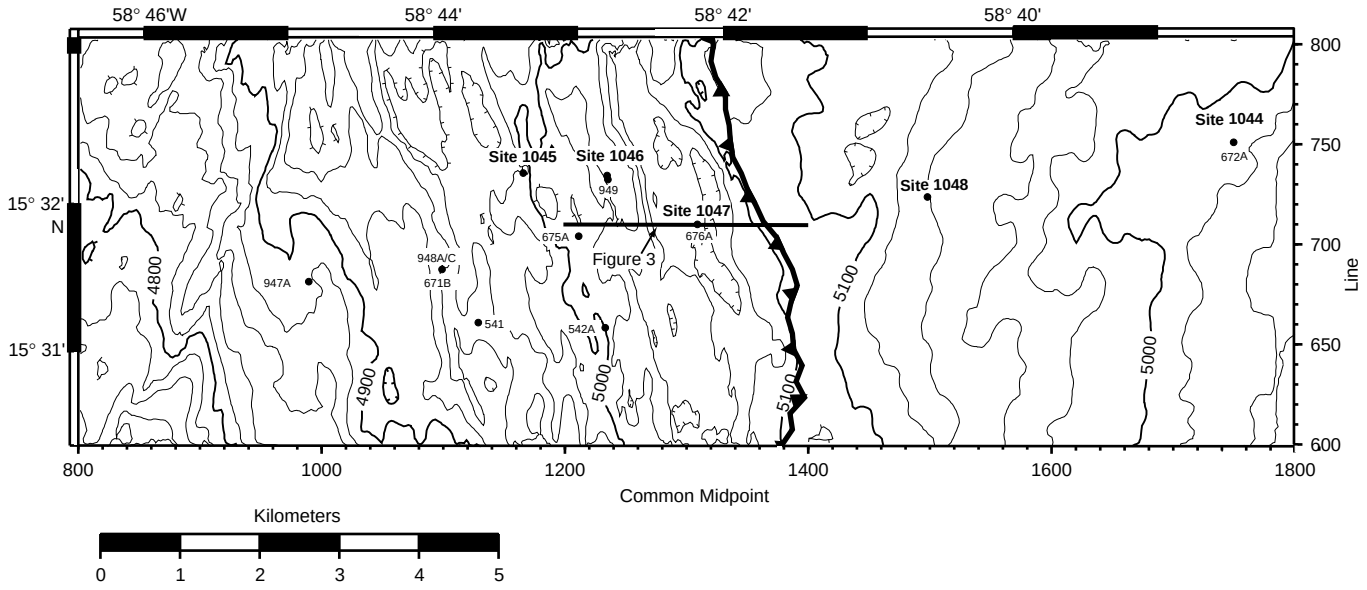

Figure 2. Bathymetric location map for Site 1047 in the Leg 171A drilling area and for previous ODP and Deep Sea Drilling Project holes in the northern Barbados accretionary prism.

low rig floor (mbrf), based on the drill pipe depth from Site 676. The actual water depth was established at 5067 mbrf (5056 m below sea level [mbsl]), based on analysis of the LWD data.

Drilling continued at 35 m/hr to 5353 mbrf (286 mbsf), where high pump pressure and high torque were encountered upon penetration of the décollement zone. The zone from 283 to 350 mbsf required considerable back reaming and hole conditioning to alleviate elevated pump pressures and torque values. Sepiolite mud sweeps (20–30 barrels) were used to condition the hole during four wiper trips through the décollement zone. Once the hole was deep enough to position the top of the bottom-hole assembly (BHA) below the décollement zone, the pump pressures and torque returned to normal. Drilling at a rate of penetration (ROP) of 35 m/hr continued without incident to 5700 mbrf (633 mbsf), at which point the allotted drilling time this hole had been expended. The drill string was pulled clear of the seafloor at 2115 hr on 5 January 1977 to end Hole 1047A.

CHARACTERIZATION OF LOGS

Definition of Log Units

The log data, with the log units labeled, are shown in Figure 4. Six log units and several subunits were defined through a combination of visual interpretation and multivariate statistical analysis (Fig. 5; see "Explanatory Notes" chapter, this volume).

Three factors were extracted from the deep resistivity, gamma-ray, thorium, potassium, photoelectric effect, bulk density, and neutron porosity logs. The three factors explain 88% of the variance contained in the data. The cluster analysis shows six prominent clusters. Table 1 summarizes the mean values and standard deviations of the log properties by cluster, each of which shows a distinct set of physical properties. Figure 5 shows the calculated cluster log, together with the log units, gamma ray, and density.

The base of log Unit 1 (0–157.9 mbsf) is defined by a negative shift in the photoelectric effect and density logs of 0.5 barns/e^- and 0.1 g/cm^3, respectively.

The base of log Unit 2 (157.9–242.2 mbsf) is characterized by a large negative shift in the resistivity, density, and photoelectric effect logs of 0.25 Ωm, 0.1 g/cm^3, and 0.4 barns/e^-, respectively.

Log Unit 3 (242.2–300.0 mbsf) is characterized by low bulk density (mean of 1.58 g/cm^3), photoelectric effect (mean of 2.5 barns/e^-), and gamma ray (mean of 64 GAPI). Subunit 3a (242.2–249.3 mbsf) is a zone of anomalously low resistivity, with values less than 0.75 Ωm in the deep resistivity. Subunit 3b (249.3–275.5 mbsf) has deep resistivity values >1.0 Ωm (Fig. 4), whereas Subunit 3c (275.5–300.0 mbsf) is another zone of anomalously low resistivity, with deep resistivity values <0.7 Ωm. The Unit 3/4 boundary is defined by positive shifts in the gamma ray, density, resistivity, and photoelectric effect. The position of the Unit 3/4 boundary is not well defined because the large shifts are at different depths on most of the logs (e.g., the density log has a positive shift at 310 mbsf, and resistivity has a positive shift at 295 mbsf).

Log Unit 4 (300.0–492.9 mbsf) is an interval of high gamma ray (mean of 131 GAPI), bulk density (mean of 1.86 g/cm^3), and photoelectric effect (mean of 3.34 barns/e^-). The base of Subunit 4a (300.0–398.8 mbsf) is seen most clearly in the cluster analysis (Fig. 5). The Subunit 4a/4b boundary is also defined by an increase in variability in the gamma ray. The base of Subunit 4b (398.8–452.8 mbsf) is at a decrease in photoelectric effect variability and a decrease in mean photoelectric effect from 3.4 to 2.9 barns/e^-. The base of Subunit 4c (452.8–492.9 mbsf) is at the top of an inferred turbidite sequence. At the Unit 4/5 boundary, there is a significant increase in the standard deviation of the resistivity and gamma-ray logs of 0.04 Ωm and 2.7 GAPI, respectively.

Log Unit 5 (492.9–562.4 mbsf) is a zone of numerous high spikes in resistivity and density and low spikes in gamma ray. The base of log Unit 5 is characterized by a decrease in variability in the resistivity and gamma-ray logs. Log Unit 6 (562.4–618.7 mbsf) is characterized by a decrease in variability in the resistivity, gamma-ray, density, and photoelectric effect logs.

LWD Log Quality

For Hole 1047A, an ROP (1.5 m averaged) of 35 m/hr was chosen because we concluded that the spectral gamma-ray data collected by the natural gamma-ray tool (NGT) at 30 to 40 m/hr penetration rates are reliable in this hole (see "Characterization of Logs" section, "Site 1044" chapter, this volume). An ROP of ~35 m/hr was maintained throughout Hole 1047A (Fig. 6).

The differential caliper values in Hole 1047A show standoffs of <1 in, except for an interval at 0–7 mbsf (up to 1.17 in), a few intervals at 246–275 mbsf (up to 1.13 in), and at 473 mbsf (1.11 in). Zones

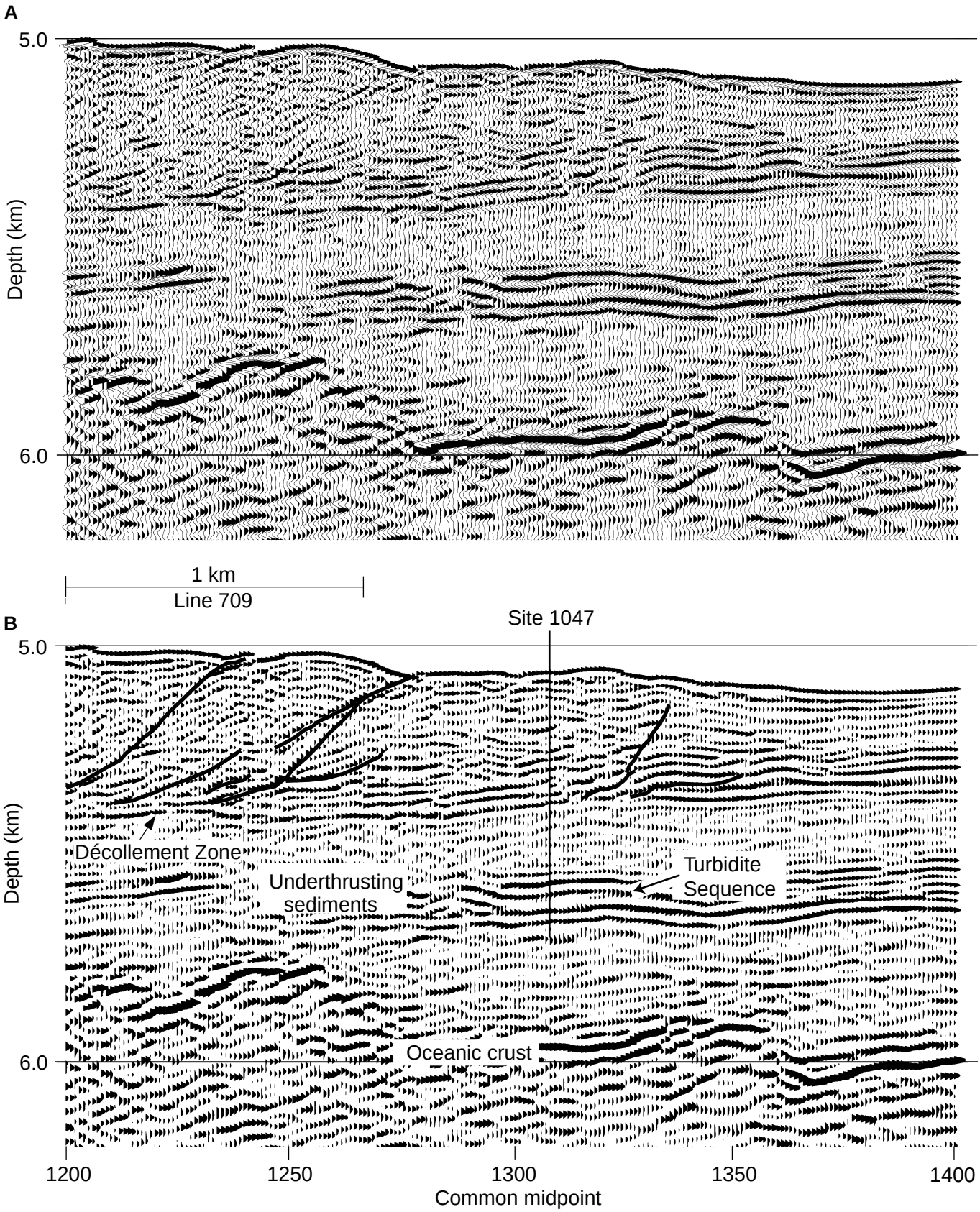

Figure 3. (**A**) Uninterpreted and (**B**) interpreted seismic Line 709 through Site 1047 (see Fig. 2 for location). Black is positive polarity; white is negative polarity. Several small thrust faults show on the interpreted section, but none are present through Site 1047. Other faulting below seismic resolution must account for much of the thickening of the section.

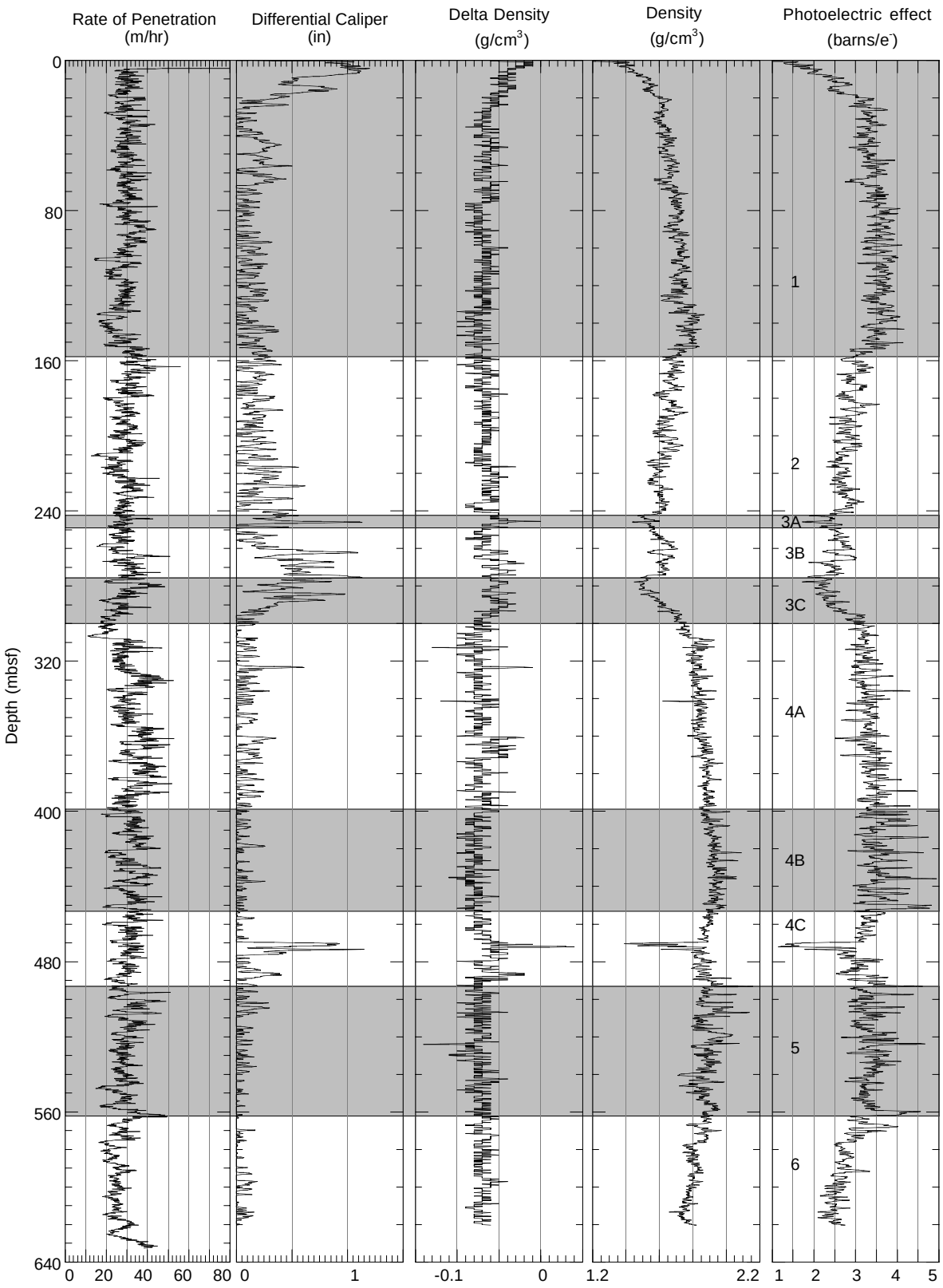

Figure 4. Site 1047 LWD data and log units. Post-cruise processed log data are available on CD-ROM (back pocket, this volume).

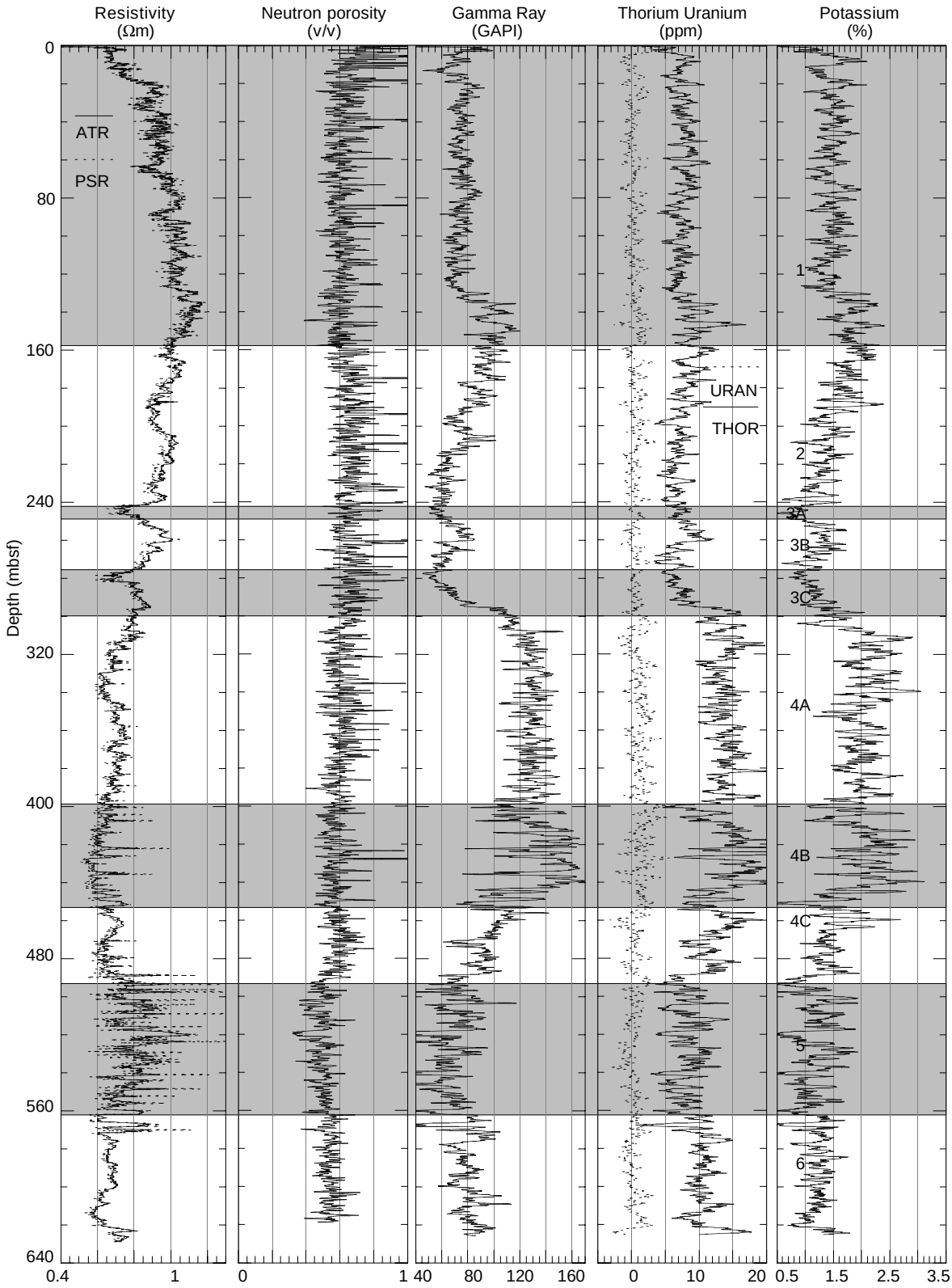

Figure 4 (continued).

Table 1. Mean values and standard deviations of the log properties according to each cluster for Hole 1047A.

	ATR (Ωm)		GR (GAPI)		THOR (ppm)		POTA (%)		PEF (barnes/e⁻)		ROMT (g/cm³)		TNPH (v/v)	
	Mean	SD	Mean	SD	Mean	SD	Mean	SD	Mean	SD	Mean	SD	Mean	SD
Cluster 1	0.82	0.15	90.2	27.6	9.8	3.4	1.53	0.45	3.2	0.5	1.767	0.123	0.6	0.07
Cluster 2	0.96	0.05	82.8	10.8	8.3	1.6	1.61	0.26	3	0.2	1.653	0.04	0.65	0.04
Cluster 3	1.01	0.05	80.4	12.3	8	1.7	1.55	0.26	3.5	0.2	1.712	0.053	0.6	0.04
Cluster 4	0.87	0.09	64.2	8	6.7	1.4	1.16	0.23	2.5	0.3	1.587	0.046	0.67	0.06
Cluster 5	0.68	0.04	131.2	15	14.4	2.3	2.08	0.34	3.3	0.3	1.884	0.058	0.8	0.05
Cluster 6	0.67	0.04	88.8	15	11	1.8	1.35	0.22	2.9	0.4	1.833	0.053	0.58	0.04
Cluster 7	0.8	0.09	67.7	17.7	7.5	2.2	1.06	0.31	3.6	0.4	1.904	0.067	0.49	0.05

Notes: SD = standard deviation; ATR = deep resistivity; GR = gamma ray; THOR = thorium; POTA = potassium; PEF = photoelectric effect; ROMT = density (rotationally processed); TNPH = thermal neutron porosity.

of minor washout are identified in the intervals 0–20, 260–290, and 470–475 mbsf. Overall, borehole conditions are excellent; 98.9% of the hole showed a differential caliper of <1 in, and 93.9% showed values <0.5 in. The bulk density correction (DRHO) varies from –0.14 to 0.04 g/cm^3, indicating that high-quality density measurements were obtained. Time-after-bit (TAB) measurements are 10 to 40 min for resistivity and gamma-ray measurements, and 30 to 80 min for density and neutron porosity measurements. Wiper trips show high TAB values of as much as 200 min in the interval 270–282 mbsf, as much as 100 min in the interval 282–295 mbsf, as much as 320 min in the interval 340–355 mbsf, as much as 90 min in the interval 360–370 mbsf, and as much as 80 min in the interval 388–400 mbsf. The wiper trip intervals from 270 to 295 mbsf coincide with part of the minor washout interval at 260–290 mbsf; however, the differential caliper and DRHO logs indicate that borehole conditions did not deteriorate significantly during the wiper trips (i.e., between the time of drilling and the time of measurement).

LOGS AND LITHOLOGY

Site 1047 is located ~29 m along an azimuth 150° from Site 676. The three lithologic units defined at Site 676 are described briefly below (Fig. 7).

Site 676

Lithologic Unit I (0–162.2 mbsf)

Lithologic Unit I comprises Pleistocene to upper Miocene calcareous mud/mudstone, calcareous clay/claystone, marl/marlstone, and volcanic ash. Moderate to intense bioturbation occurs throughout the unit. Most of the volcanic ash has been completely disrupted by burrowing. The carbonate content decreases downward through Unit I, grading into the predominantly noncalcareous sediments of Unit II.

X-ray-diffraction (XRD) analysis of sediments from Unit I shows that, in addition to relatively high percentages of calcite, there is also a variable plagioclase content, which reflects the presence of ash layers. Quartz content is low overall, and clay content varies widely between 3% and 70%.

Lithologic Unit II (162.2–262.7 mbsf)

Subunit IIA consists of homogeneous claystone and mudstone with intervals of slightly calcareous to calcareous claystone and mudstone. Subunit IIB consists of claystone and mudstone containing local trace amounts of radiolarians. The presence of siliceous biogenic detritus distinguishes Subunit IIB from Subunit IIA. All of the Unit II sediments contain common volcanic ash, both as highly bioturbated layers and as a minor disseminated constituent of the sediment.

Clay mineral content in Unit II is much higher than that in Unit I, varying from 77% to 92%. Plagioclase and quartz are generally minor constituents (<15% each). XRD analysis shows little calcite in the Unit II sediments.

Lithologic Unit III (262.7–310 mbsf)

Lithologic Unit III consists of lower Miocene siliceous mudstone, slightly siliceous mudstone, claystone, and volcanic ash. These sediments contain between 2% and 25% radiolarians and sponge spicules. Local minor color mottling occurs throughout this unit, which closely resembles portions of the décollement zone recovered at Site 671.

Unit III is similar to Unit II in terms of bulk mineralogy, although the former is slightly less clay rich overall. The decrease in clay content is balanced by an increase in quartz content.

Correlation With Log Units

Log Unit 1 (0–157.9 mbsf) is characterized by high photoelectric effect, increasing density with depth, and low and relatively constant gamma ray. The observed log characteristics in this uppermost unit are similar to those from Sites 1044 and 1046. High photoelectric effect readings and low gamma-ray readings suggest that log Unit 1 corresponds to lithologic Unit I at Site 676, which has a high carbonate content (Fig. 7). The observed increase in density throughout the unit is interpreted as a normal compaction trend.

Compared with log Unit 1, log Unit 2 (157.9–242.2 mbsf) is characterized by a general decrease in resistivity, a decrease in gamma ray, and a lower and decreasing photoelectric effect. Density also decreases throughout the unit. The gradual decrease in gamma ray, resistivity, and photoelectric effect is thought to be caused primarily by an increase in porosity as well as a decrease in carbonate content. This log unit corresponds to lithologic Subunit IIA, which comprises homogeneous claystones and mudstones, with intervals of calcareous claystones and mudstones.

The wide variations in log responses within log Unit 3 are caused by a combination of lithologic and structural features. Log Subunit 3a (242.2–249.3 mbsf) correlates with the top of lithologic Subunit IIB at Site 676. The low photoelectric effect and gamma-ray log responses are typical of the slightly siliceous, clay-rich sediments that characterize lithologic Subunit IIB. The low density and resistivity suggest that the interval defined as log Subunit 3a is a high-porosity zone. This interval correlates with a thrust fault seen in the seismic profiles (see “Logs and Structure” section, this chapter).

Log Subunit 3b (249.3–275.5 mbsf) also correlates with lithologic Subunit IIB but differs from the overlying log subunit in that it represents relatively undisturbed sediment. Structural data from Site 676 indicate that faulted and deformed zones over- and underlie this stratigraphic interval (Shipboard Scientific Party, 1988b). Log Subunit 3c correlates with the radiolarian-rich sediments of lithologic Unit III. The low resistivity and gamma-ray logs within this interval indicate that log Subunit 3c also correlates with the décollement zone as structurally defined in the cores. The log signature at the décollement zone at Site 1047 is similar in shape and amplitude to the equivalent interval logged at Sites 1044, 1045, and 1048.

Log Units 4 and 5 correlate with the interbedded lithology found in the upper section of the underthrust sediments at Sites 672 and 671.

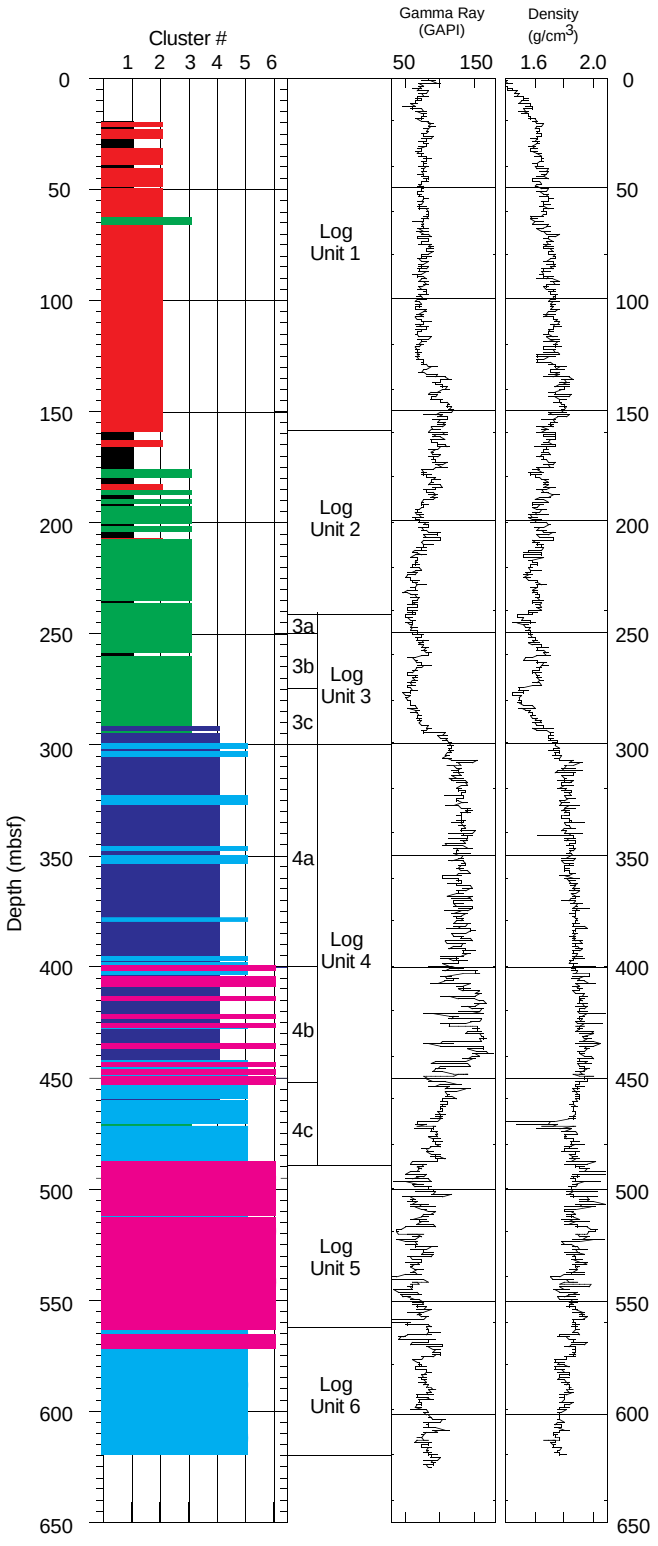

Figure 5. Definition of log units for Site 1047. Six clusters were derived from three factor logs that account for 88% of the total variance observed in the data. Boundaries between first-order log units correspond to changes in log character related primarily to lithology that are clearly visible on logs (e.g., gamma ray, density, photoelectric effect, and resistivity). Second-order units represent subtle changes in log character that are observed in only a few curves and that may not be related to lithology.

These sediments typically show high variability in log response. The spiky nature of the photoelectric effect and gamma-ray logs evident in log Subunits 4a and 4b suggests interbedding of compositionally different sediments. Interbedded claystones, siltstones, and marls are observed in the equivalent section of lithologic Unit III at Site 672. The downward increase in amplitude of the photoelectric effect and gamma-ray curves through Subunits 4a and 4b is probably related to an increase in the calcite component, based on the core description and XRD analysis from Site 672. Log Subunit 4c (452.8–492.9 mbsf) is characterized by decreasing gamma ray, photoelectric effect, and density. This trend is indicative of a decrease in calcite, which is consistent with a low-calcite interval found in the upper Eocene sediments at Site 672. A sharp negative peak in photoelectric effect and density at ~472 mbsf appears to correlate with a thick, sandy, quartz-rich bed within the upper Eocene at Site 672. Log Unit 5 (492.9–562.4 mbsf) is characterized by variable resistivity, gamma ray, photoelectric effect, and density. This unit displays log characteristics similar to those of the turbidite unit penetrated at Sites 1044 and 1046.

Log Unit 6 (562.4 mbsf to total depth) is characterized by decreasing photoelectric effect and density and increasing and variable gamma ray. This unit correlates with the lower Eocene noncalcareous claystones and siliceous claystones recovered at Sites 672 and 543.

LOGS AND STRUCTURE

Site 1047 is located ~29 m from Hole 676A, cored during Leg 110. Structural features interpreted from the seismic reflection data are correlatable between holes, making the comparison of core data to LWD data reasonable. This section compares structural features in core, seismic, and LWD data, which are summarized in Figure 8.

Core recovery was good (84.5%) in Hole 676A, where core deformation structures consist of scaly fabric, sediment-filled veins, and discrete normal and reverse faults (Shipboard Scientific Party, 1988a). Cores show a thrust fault at 210 mbsf, which is marked by intense subhorizontal scaly fabric at the base of a section, with a relatively high degree of deformation from 150 to 210 mbsf. This highly deformed interval is within log Unit 2. This fault correlates with a gamma-ray anomaly and an inversion in resistivity. Other LWD logs show no discernible perturbation at 210 mbsf. A similar resistivity inversion is located at the top of log Unit 2, where subhorizontal scaly fabrics were noted in the core but were not attributed to a fault. We interpret this feature as a fault. It is significant that log Subunit 3a correlates with a zone of low core recovery. Such low recovery may have been because of the presence of highly deformed material in that interval, which, in turn, could account for the LWD log anomalies associated with log Subunit 3a. A thrust fault at 291 mbsf is defined by a biostratigraphic inversion and is in a zone of subvertical mud-filled veins from 271 to 305 mbsf. These veins were interpreted by the Shipboard Scientific Party (1988b) as indicative of incipient subhorizontal shear, and the zone from 271 to 305 mbsf was identified as the décollement zone. This zone correlates with the bottom portion of log Unit 3, characterized by an increase in caliper, a reversal in the trend of density and photoelectric effect, an inversion in resistivity, and an abrupt increase in gamma-ray counts. The seismic data show the décollement zone at about 300 mbsf (see “Background and Objectives” section, this chapter)

LOGS AND PHYSICAL PROPERTIES

Discussed in this section are the LWD results that are relevant to the physical properties at Site 1047. The density characteristics downhole, as inferred from the density and photoelectric effect logs, are described in detail and are compared with index physical proper-

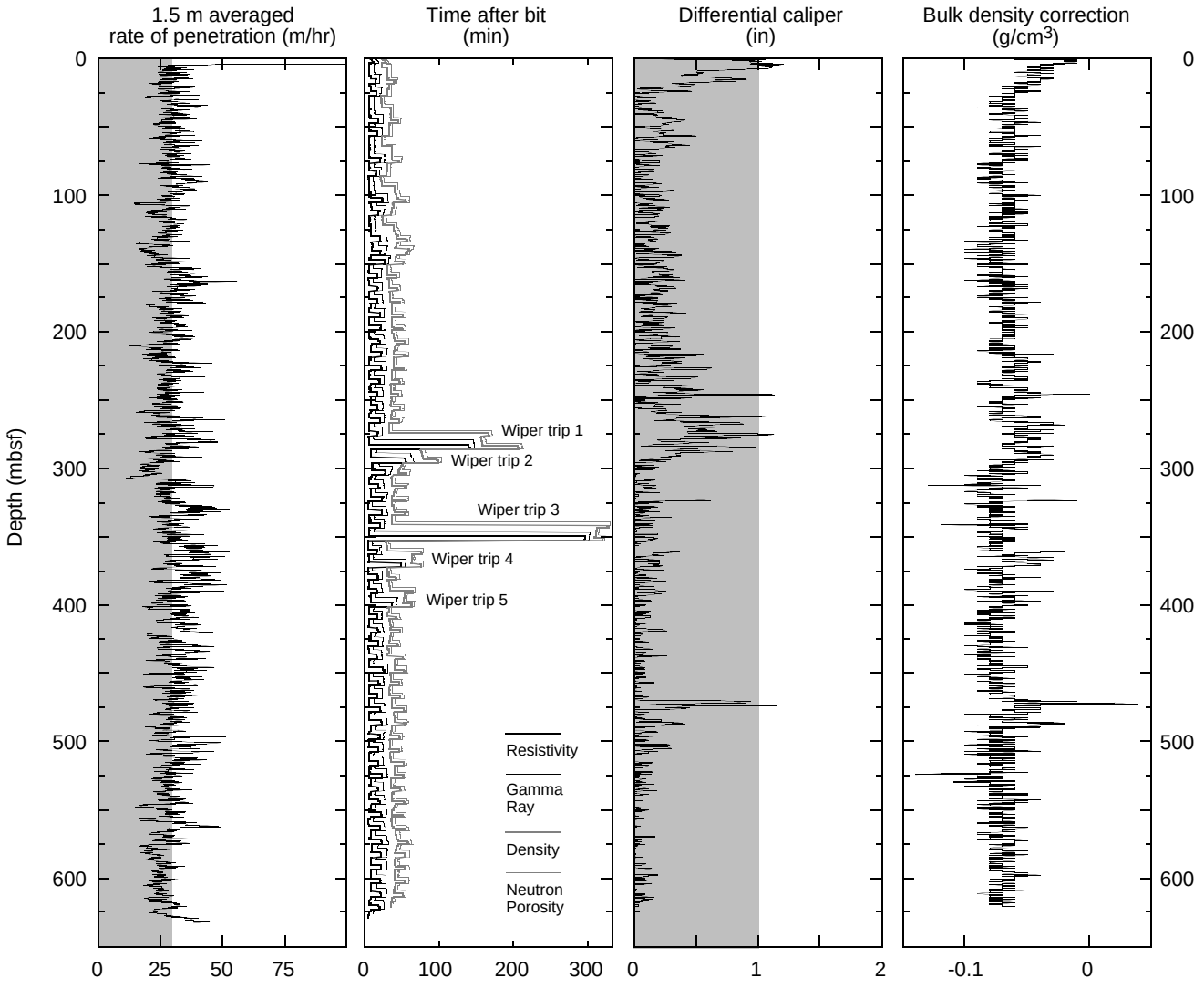

Figure 6. Summary of the quality-control logs. The shaded area in the rate of penetration column shows the reliable zone for NGT measurements according to industry experience. The shaded area in the differential caliper column indicates good borehole conditions.

ties measurements on cores from Site 676, where sediments were recovered at the same location during Leg 110. The density and resistivity profiles across the décollement zone at Site 1047 are compared for possible correlation to the corresponding interval at reference Site 1044.

Density

The downhole density increase between 0 and 125 mbsf (Fig. 9A) follows a normal consolidation trend. An offset toward higher density values (approaching 1.9 g/cm^3) occurs in the interval between 125 and 140 mbsf, followed by a change to an irregular downhole trend with decreasing density values that end abruptly at 221 mbsf. At this depth, density is offset sharply to even lower values (below 1.5 g/cm^3). Between 221 and 237 mbsf, density values rise with some excursions to about 1.65 g/cm^3, below which they decrease again to about 1.5 g/cm^3. In the interval from 237 to 275 mbsf, density values again increase in an irregular fashion, then drop sharply to about 1.43 g/cm^3. Between 275 and 310 mbsf, density values show a steep increase downhole to a peak value of 1.8 g/cm^3. This interval coincides with the structurally defined décollement zone (271–305 mbsf). It is also characterized by a concurrent gradual lithologic change that is probably partly responsible for the significant increase in bulk density. From 310 to 450 mbsf, density values rise again in a steady trend, approaching an apparently normal consolidation trend. From 450 mbsf to total depth in Hole 1047A, density values decrease slightly, with strong excursions that are correlated with turbidite layers. An interval of anomalously low densities occurring at about 470 mbsf correlates with differential caliper readings that exceed 1 in and is not believed to represent actual conditions. Comparison of the Site 1047 density log data and the core data from Site 676 shows a remarkable correlation of both data sets (Fig. 10).

Photoelectric Effect

As expected, the photoelectric effect log closely resembles the pattern seen in the density log (Fig. 11). Therefore, the depths of intervals and offsets described for the density log also broadly apply to the photoelectric effect log.

Resistivity Logs

The character of the resistivity log above the décollement zone at Site 1047 is similar to the character of the density curve (log Units 1

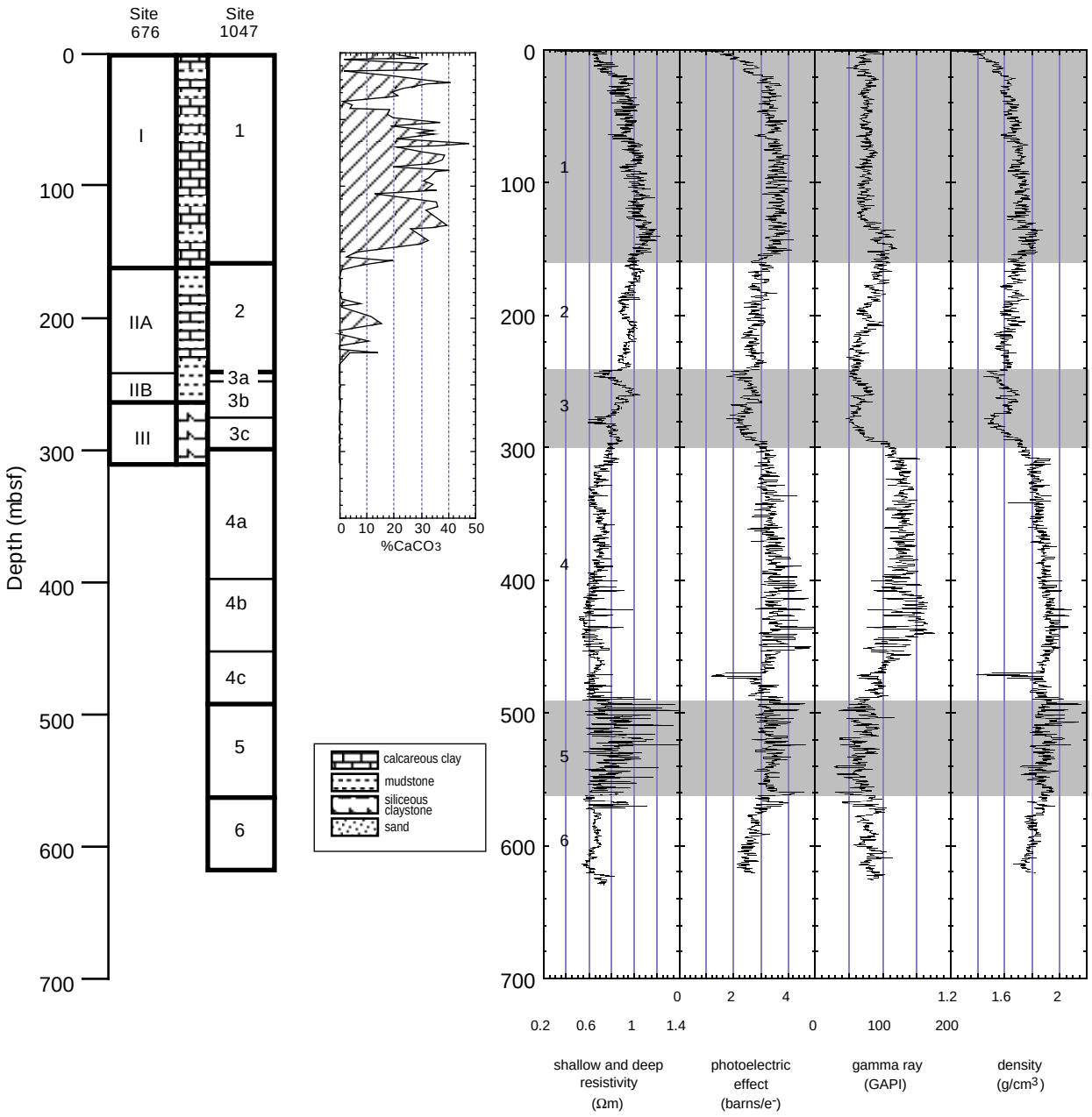

Figure 7. Summary of Site 1047 log units and Site 676 lithology data. The lithology column summarizes the major lithologic units described for Site 676 (Shipboard Scientific Party, 1988b). The percentage of carbonate shows the compositional variation among the lithologic units. Shaded areas in the log plots represent the boundaries of the major log units. The dark curve in the resistivity column is the shallow resistivity; the light curve is the deep resistivity.

and 2). Below the décollement zone, the resistivity trend differs greatly from the density trend. Overall, the deep and shallow resistivities increase to 1.15 Ωm at 140 mbsf and then begin a gradual decrease to 0.55 Ωm at 430 mbsf.

The décollement-zone signature at Site 1047 is unique. It has a 0.2-Ωm decrease in resistivity at the top and bottom of the zone (log Subunits 3a and 3c), with resistivity values as much as 1.0 Ωm in the middle of the zone. There is a gradual decrease in resistivity from 0.8 to 0.65 Ωm in log Unit 4 (300.0–492.9 mbsf). The shallow resistivity in log Unit 5, the inferred turbidite section, has a high standard deviation resulting from thin turbidite beds of varying resistivity. The overall resistivity increases by about 0.1 Ωm in log Unit 5 and then decreases by 0.15 Ωm in log Unit 6.

Comparison of the Décollement Zone at Sites 1044 and 1047

To examine the change in physical properties as sediments are loaded by accretion, density, and resistivity from the décollement zone at Site 1047 were compared with those at Site 1044 (Fig. 12). The same scale was used for Figures 10, “Site 1045” chapter (this volume), and Figure 13, “Site 1046” chapter (this volume), to facilitate a four-site (1044 through 1047) comparison. Correlation of Site 1047 with the reference site relied on identification of the top of the radiolarian-rich unit at ~170 mbsf at Sites 672 and 1044 (Shipboard Scientific Party, 1988a) and ~270 mbsf at Sites 676 and 1047 (Shipboard Scientific Party, 1988b). In general, the décollement zone at

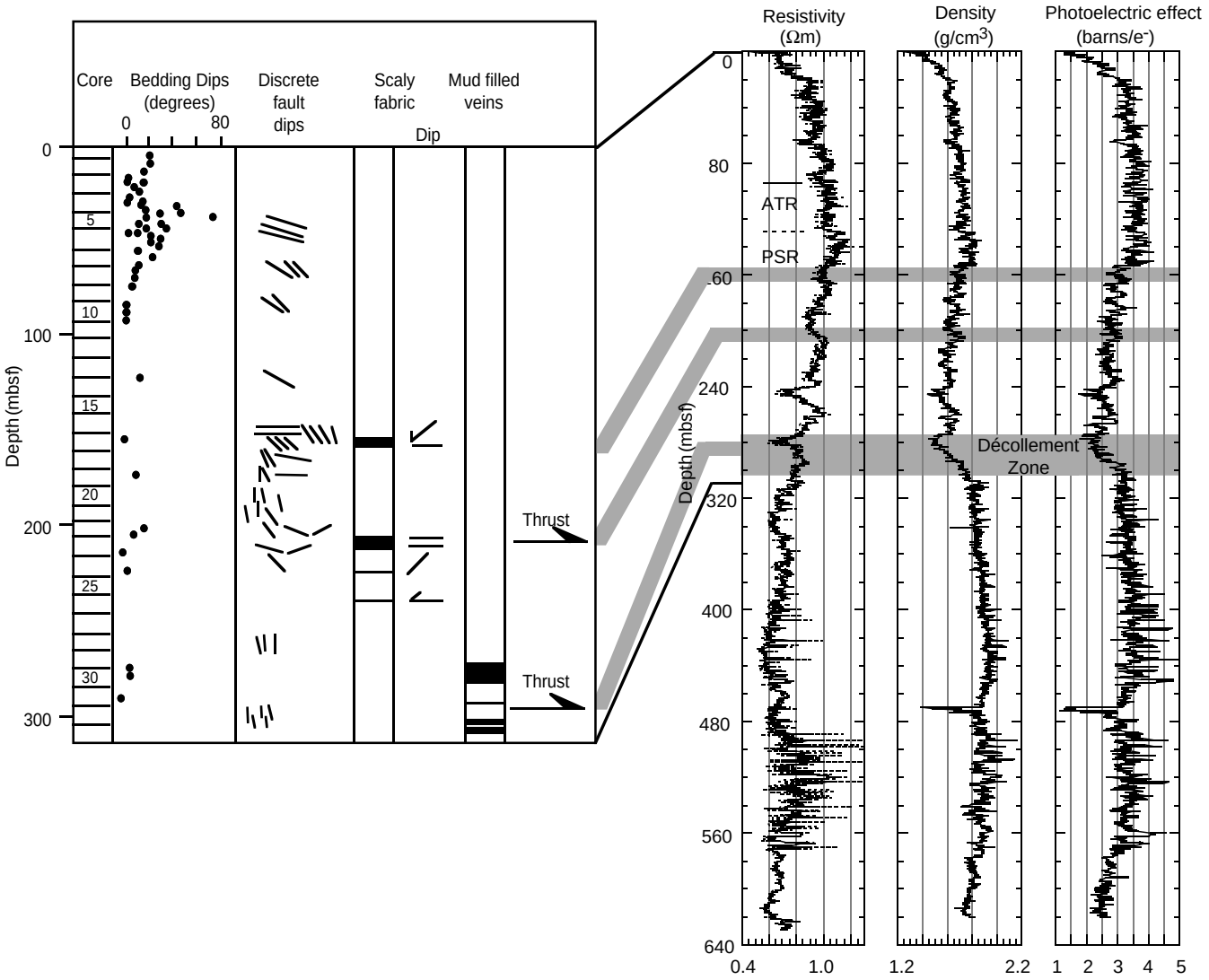

Figure 8. Structural synthesis of faults identified in Hole 676A cores and in Hole 1047 LWD logs.

Site 1047 has higher density values than that at Site 1044 and lower density values than that at Site 1046 (Fig. 13, "Site 1046" chapter, this volume). This comparison suggests a consistent increase in density over time and in loading by the overlying prism. Site 1045 (Fig. 10, "Site 1045" chapter, this volume) does not fit the trend; it has an average density less than that measured at Site 1046.

Comparison of the Underthrust Section at Sites 1047 and 1044

The density, resistivity, and photoelectric effect logs from the underthrust section are similar to their counterparts from reference Site 1044. This similarity may indicate either lack of compaction of the underthrust sediments or compaction masking by lateral facies changes.

Summary

1. The density log agrees well with bulk densities of core from Site 676.
2. Density, resistivity, and photoelectric effect logs show a discontinuity at about 125 mbsf, below which all decrease down to the inferred décollement zone at 271 mbsf.
3. At the structurally defined décollement zone (271–305 mbsf), the density is higher than at the proto-décollement zone at Site 1044, and it fits a trend of increasing décollement-zone density from Site 1044 westward to Site 1046.
4. Density, resistivity, and photoelectric effect logs from the underthrust sediments are similar to those from the corresponding section below the proto-décollement zone at Site 1044.

LOGS AND INDICATORS OF FLUID FLOW

At Site 1047, LWD was used to collect continuous data at a site (Site 676) where previous drilling found geochemical and thermal evidence for active fluid flow. Results of transient thermal modeling suggest that recent flow (20 to 30 yr ago) occurred along a fault zone at 32 mbsf (Fisher and Hounslow, 1990). High methane values suggest the presence of fluid flow horizons at about 40, 200, and 280

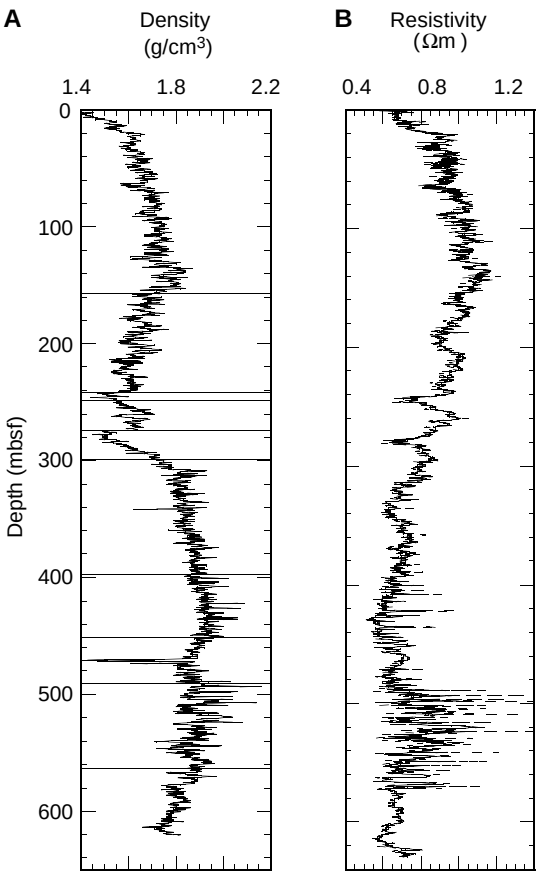

Figure 9. (**A**) Density and (**B**) resistivity (deep = solid line, shallow = dashed line) vs. depth in Hole 1047. Horizontal lines encompass intervals discussed in the text (log unit boundaries).

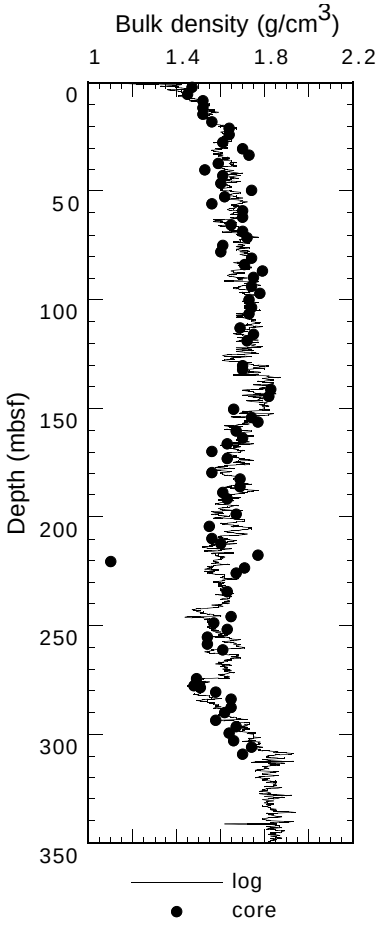

Figure 10. Density vs. depth in Hole 1047A compared with core wet bulk densities from Site 676.

mbsf, whereas low (below-seawater) chloride values suggest fluid advection at about 250 mbsf. Figure 1 shows the geochemical data from Site 1047, together with the density, gamma-ray, and resistivity LWD logs. In this section, we discuss the LWD results from proposed fluid-flow horizons.

Thrust Faults

Although not particularly distinctive, decreases in the resistivity and density logs observed at ~30 mbsf may be associated with a possible zone of deformation observed in the cores from 25 to 52 mbsf (Shipboard Scientific Party, 1988b). This correlates well with the observed high methane values at 33 mbsf and the thermal anomaly observed at 32 mbsf. However, no low-chloride signature was observed at this depth.

A zone of deformation was described in the Site 676 cores from 199 to 223 mbsf (Shipboard Scientific Party, 1988b); this correlates with a methane high observed at 190 mbsf. The LWD data show a zone of low resistivity from ~190 to 205 mbsf, but no change in the density log is observed at this depth.

At 250 mbsf both shear fabrics and a low-chloride anomaly were found at Site 676. A thrust fault at 250 mbsf is imaged in the seismic data, and low values are also present in the density and resistivity logs at this depth. Although no methane anomaly is found here, the chloride data suggest that there has been fluid flow along this fault.

Décollement Zone

The top of the décollement zone at Site 1047 correlates with decreases in the density and resistivity logs at 280 mbsf. At this depth, a negative polarity reflector is imaged on the seismic profiles (see "Logs and Seismic Data" section, this chapter). A methane anomaly was found at 286 mbsf, slightly below the low-density, low-resistivity zone. In addition, there was a broad zone of high caliper log values at this depth.

The radiolarian-rich horizon that correlates with the proto-décollement zone at Sites 672 and 1044 was found at Site 676, from 275 mbsf to the bottom of the hole (310.2 mbsf). Using this radiolarian-rich zone to correlate horizons, it is possible to compare densities within the décollement zone at Sites 676 and 1047 and the proto-décollement zone at Sites 672 and 1044 (see "Physical Properties" section, this chapter; Fig. 12). From the density profiles, consolidation intermediate between that of Hole 1044A and Hole 1046A (Fig. 13, "Site 1046" chapter, this volume) can be inferred for Hole 1047A, suggesting a consistent relationship of increasing consolidation with increasing time and loading. Hole 1045A (Fig. 10, "Site 1045" chapter, this volume) is a notable exception to the trend, showing density intervals that are nearly as low as those observed within the Site 1044 proto-décollement zone (see "Logs and Indicators of Fluid Flow" section, "Site 1045" chapter, this volume).

Underthrust Sediments

A temperature gradient of 60°C/km was recorded at the base of the hole at Site 676. There is no thermal anomaly associated with the décollement zone. Thus, it appears that the same pattern of heat flow found at Sites 672 and 949 is also present at Site 1047. The thermal data are best explained by migration of warm fluids along the turbidite horizons below the base of the hole at Site 676. There is a large

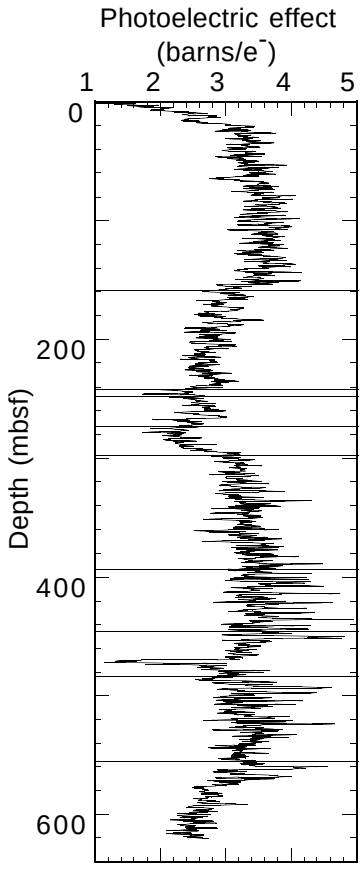

Figure 11. Photoelectric effect vs. depth in Hole 1047A. Lines represent intervals discussed in the text (log unit boundaries).

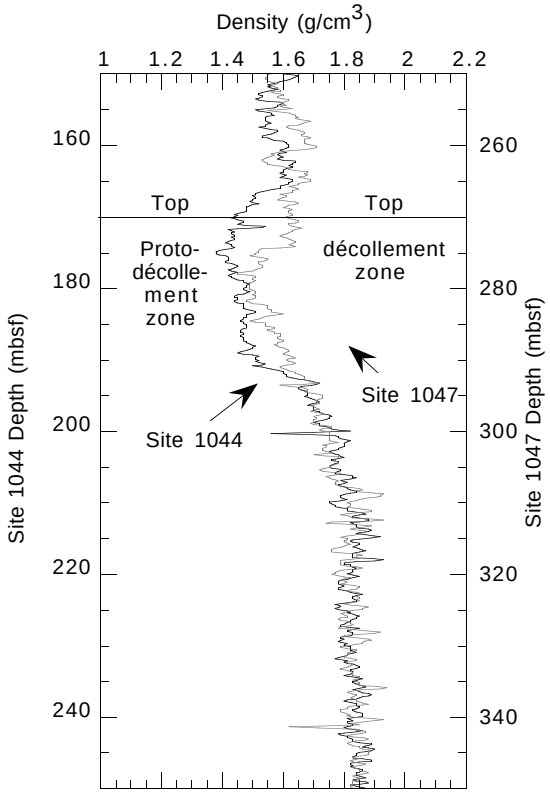

Figure 12. Comparison of density across the décollement zone at Sites 1044 and 1047.

increase in the caliper log in the turbidite section of this hole. However, because there are sands throughout the turbidite section that do not correspond to high caliper-log values, it seems unlikely that this increase is caused solely by sandy lithology.

Summary

1. Although signatures correlated with known fluid migration horizons can be found within the LWD logs, these signatures are not necessarily unique (i.e., not every density/resistivity offset denotes a fluid migration pathway).
2. Densities within the décollement zone reflect increasing consolidation with loading and time for Sites 1044, 1046, and 1047. Site 1045 is an exception to this trend, suggesting that it is hydrogeologically unique.

LOGS AND SEISMIC DATA

From the density log we constructed the synthetic seismogram shown in Figure 13. A linear velocity profile was used and the synthetic seismogram was constructed as described in the "Explanatory Notes" chapter (this volume). The gradient used to construct the velocity profile was the same one used at Sites 1044 through 1046.

Above the décollement zone, the synthetic trace shows significant discrepancies among the traces on either side of common midpoint 1308, where Site 1047 was drilled. The arrival times are not well matched, and several large-amplitude events in the 100 m above the décollement zone do not appear on the actual data. One of these events could be sufficiently close to the décollement zone to affect the waveform. The décollement zone is a weak reflection at this site, much smaller than at Site 1045 and only slightly larger than reflections from within the accretionary wedge. In the synthetic trace, the amplitude is close to twice that of the actual data. The large amplitude of the décollement-zone reflection in the synthetic trace appears reasonable given that it is caused by a distinct low-density (1.5 g/cm^3) interval, and it remains uncertain why there are such distinct differences between the data and the synthetic trace at and above the décollement zone.

Below the décollement zone there is a reasonably good correlation between the synthetic trace and the data. The nonreflective intervals between 5400 and 5550 mbsl correspond well with respect to the data and the synthetic trace. The reflective interval in the bottom 200 m of the synthetic trace is also reasonably matched in amplitude and arrival time. We speculate that the synthetic seismogram matches the actual data below the décollement zone better than above because either (1) acoustic impedance changes above the décollement zone are dominated by velocity changes that are not included in our smooth velocity model, whereas all acoustic impedance changes below the décollement zone are determined by density changes; or (2) the logged densities below the décollement zone are laterally continuous, whereas those above the décollement zone are not laterally continuous (see "Seismic Resolution and Core-Log-Seismic Correlation" section, "Explanatory Notes" chapter, this volume).

REFERENCES

Fisher, A.T., and Hounslow, M.W., 1990. Heat flow through the toe of the Barbados accretionary complex. *In* Moore, J.C., Mascle, A., et al., *Proc.*

ODP, Sci. Results, 110: College Station, TX (Ocean Drilling Program), 345–363.

Shipboard Scientific Party, 1988a. Site 672. *In* Mascle, A., Moore, J.C., et al., *Proc. ODP, Init. Repts.*, 110: College Station, TX (Ocean Drilling Program), 205–310.

————, 1988b. Site 676. *In* Mascle, A., Moore, J.C., et al., *Proc. ODP, Init. Repts.*, 110: College Station, TX (Ocean Drilling Program), 509–573.

Ms 171AIR-106

NOTE: For all sites drilled, shore-based log processing data are available on CD-ROM. See Table of Contents for material contained on CD-ROM.

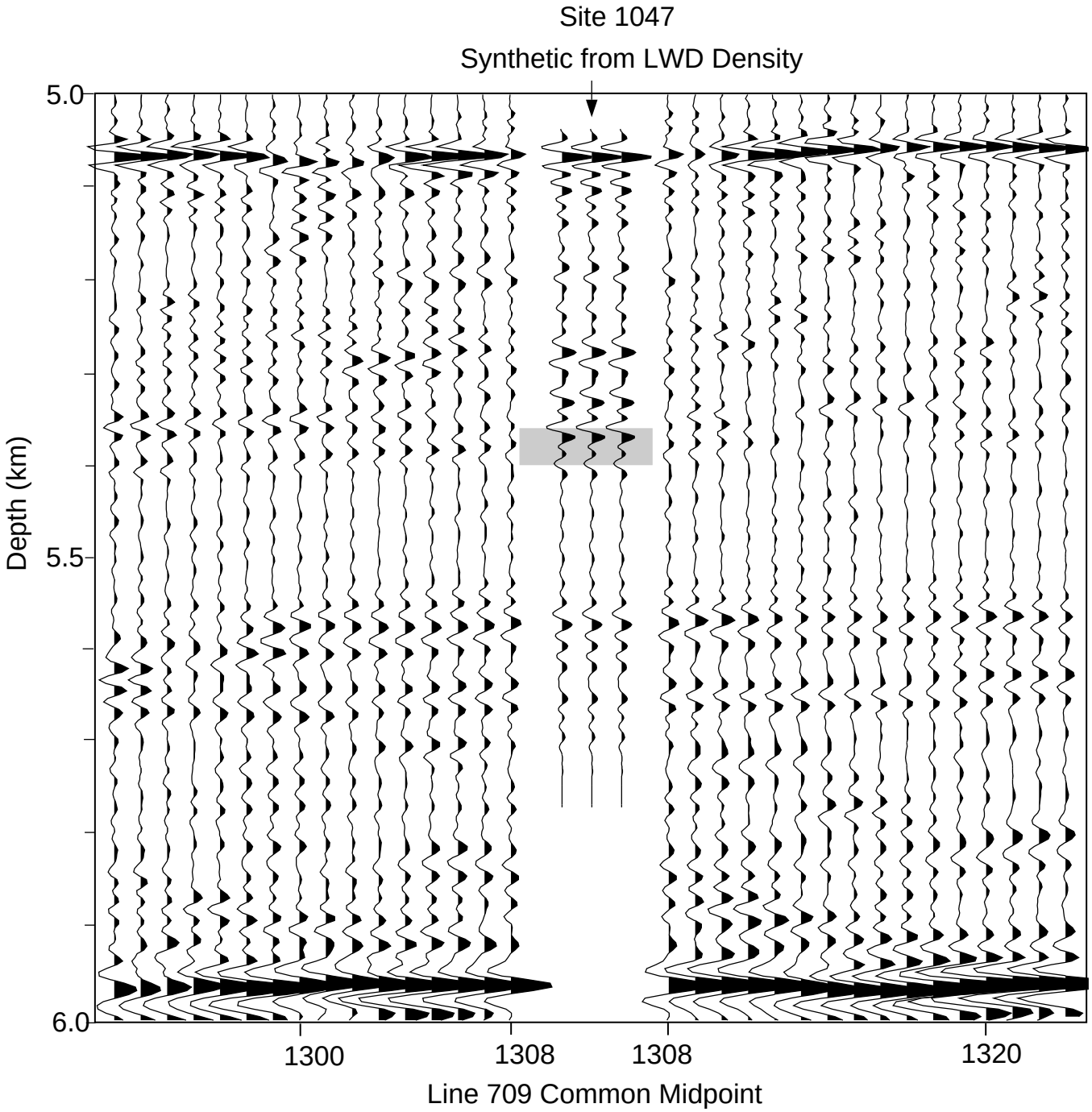

Figure 13. Three identical synthetic traces are shown at Site 1047 on Line 709. See "Explanatory Notes" chapter (this volume) for description of the synthetic seismogram construction. The shaded area shows the location of the décollement zone, as indicated by the density log. Trace spacing is 15 m; horizontal exaggeration is 2×.